

Spherical-Wave Model for Short-Range MIMO

Jeng-Shiann Jiang, *Member, IEEE*, and Mary Ann Ingram, *Senior Member, IEEE*

Abstract—The plane-wave assumption has been used extensively in array signal processing, parameter estimation, and wireless channel modeling to simplify analysis. It is suitable for single-input single-output and single-input multiple-output systems, because the rank of the channel matrix is one. However, for short-range multiple-input multiple-output (MIMO) channels with a line-of-sight (LOS) component, the plane-wave assumption affects the rank and singular value distribution of the MIMO channel matrix, and results in the underestimation of the channel capacity, especially for element spacings exceeding half a wavelength. The short-range geometry could apply to many indoor wireless local area network applications. To avoid this underestimation problem, the received signal phases must depend precisely on the distances between transmit and receive antenna elements. With this correction, the capacity of short-range LOS MIMO channels grows steadily as the element spacing exceeds half a wavelength, as confirmed by measurements at 5.8 GHz. In contrast, the capacity growth with element spacing diminishes significantly under the plane-wave assumption. Using empirical fitting, we provide a threshold distance below which the spherical-wave model is required for accurate performance estimation in ray tracing.

Index Terms—Channel capacity, line-of-sight (LOS), multiple-input multiple-output (MIMO), plane-wave model, ray tracing, spherical-wave model.

I. INTRODUCTION

MULTIPLE-INPUT multiple-output (MIMO) transmission is an extremely spectrum-efficient technology that uses several antennas at both ends of the communication link [1], [2]. However, it has been revealed that some factors, such as the richness of the multipath, the correlation of the entries of the channel matrix, and the keyhole effect, might degrade MIMO system performance significantly in a real environment [3], [4]. Presence of a strong line-of-sight (LOS) component is sometimes viewed as a degradation in the context of MIMO, because a strong LOS is usually thought to result in a unity-rank channel, and a unity-rank channel is incapable of supporting multiple parallel data streams.

This paper makes several claims: 1) that a LOS MIMO channel can be full rank and yield the highest possible capacity; 2) that the spherical-wave model is required to properly analyze short-range MIMO; and 3) that large antenna spacing can have a very significant and positive impact at short range. These

claims are interrelated. The full rank, as well as the impact of spacing, will not be evident in the analysis without modeling the LOS with spherical waves. Furthermore, the full rank will not be reached at some typical wireless local area network (WLAN) ranges without larger-than-usual antenna spacing.

The work was motivated by a discrepancy involving measured data. In [5], the authors attempted to estimate the path parameters of the MIMO channel for the purpose of reconstructing the matrix of MIMO channel gains for arbitrary array geometries. The path parameters included the angles of departure and arrival at the transmitter and receiver arrays, respectively. It was found that the capacity of the reconstructed MIMO channels was less than the directly measured capacity, especially for large antenna spacing. In this paper, we show that in the short-range scenarios of [5], a major reason for the discrepancy is incorrect modeling of the LOS component. Specifically, we find that computing the phases of the channel gains based on the precise distances between transmit and receive antennas, in other words, using the spherical-wave model instead of the plane-wave model, is necessary to alleviate the discrepancy. Use of the spherical-wave model for the LOS gives “richness” to even a free-space MIMO channel.

This observation was made in [6], where particular geometries were sought that could yield channel matrices with full rank. In [7], this phenomenon was investigated by simulating the free space and two-path channels, but only two orientations of the arrays were considered. They validated the phenomenon over measured channels in a parking lot with fixed antenna spacing (half-wavelength). Also using the spherical-wave model, in [8], it was shown that the capacity was sensitive to element spacing in free-space and in Rician fading channels with various K-factors. It was concluded that the sensitivity of the capacity to the element spacing is significantly reduced when the K-factor is less than 10 dB [8].

In contrast to these previous works, this paper analyzes the performance of arrays with various orientations and elevation angles in the free-space channel and in a square room with up to 20 reflections. In addition, we specify a distance threshold in units of wavelength to determine whether the plane-wave model can be used without causing significant errors. Furthermore, this paper uses a measured indoor channel to show how the more precise LOS model narrows the gap between capacities of measured and reconstructed MIMO channels, especially for larger element spacing. Moreover, because the LOS path is much stronger than the multipath, and because LOS alone can provide substantial capacity, we conclude that special care should be taken when modeling the LOS in short-range MIMO links, even when there is plenty of multipath.

Other authors have considered the effect of element spacing on MIMO capacity. Increased capacity with increased element

Paper approved by R. A. Valenzuela, the Editor for Transmission Systems of the IEEE Communications Society. Manuscript received September 16, 2003; revised March 25, 2004 and May 11, 2004. This work was supported in part by the National Science Foundation (NSF) under Grant CCR-0121565, and in part by the Georgia Tech Broadband Institute (GTBI). This paper was presented in part at the IEEE Vehicular Technology Conference, Fall, 2003.

The authors are with the School of Electrical and Computer Engineering, Georgia Institute of Technology, Atlanta, GA 30332 USA (e-mail: mai@ece.gatech.edu).

Digital Object Identifier 10.1109/TCOMM.2005.852842

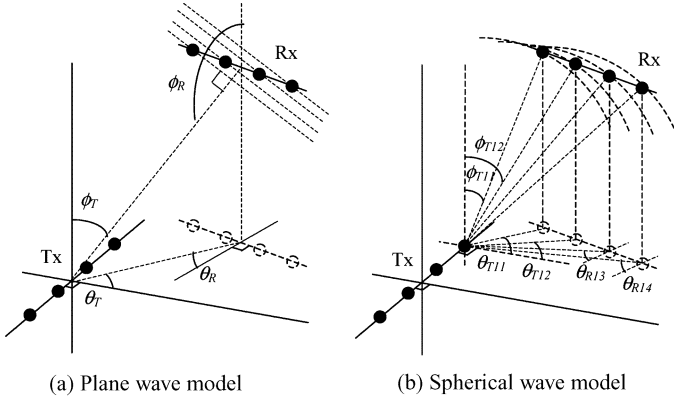


Fig. 1. Illustration of (a) the plane-wave model and (b) the spherical-wave model. Tx and Rx arrays are assumed to be parallel with the horizontal ($x - y$) plane. In the plane-wave model, the DOAs are the same for all elements in Rx, while in the spherical-wave model, the DOA of each element in Rx is different from the others.

spacing in non-LOS (NLOS) channels has been observed in simulation of stochastic geometric models with angularly clustered multipath [9]–[11], and in ray tracing [12]. The improvement in these cases is attributed to the reduction in correlation of the multipath fading across antennas [9]–[12]. Others have analyzed short-range LOS MIMO links using ray tracing, and concluded that capacity is either insensitive to spacing [13] or that half-wavelength spacing yields full capacity [14]. In [13], the plane-wave model is specified, and in [14], the LOS model is not specified. In the context of these previous works, we first note that the LOS component is unfaded, therefore the spacing effects reported here are not because of decorrelation of fading. Second, as shown here, the conclusions about spacing that follow from the spherical-wave model are different from those of [13] and [14]. Finally, in contrast to [6], this paper considers the statistics of free-space short-range MIMO capacities for array geometries and random relative orientations that might be encountered in WLAN applications. The results suggest that larger element spacing could be very beneficial for indoor WLANs using MIMO.

The paper is organized as follows. In Section II, free-space channels are considered, and the discrepancy between the plane- and spherical-wave models is demonstrated for variations in direction-of-arrival (DOA), direction-of-departure (DOD), antenna spacing, and distance between transmit array (Tx) and receive array (Rx). In Section III, we use ray-tracing to simulate the multipath phenomenon in a square room. The performances of these models are compared based on a Monte Carlo approach. In Section IV, we briefly describe our MIMO measurement system and show the measurement results to validate the importance of the spherical-wave model in the MIMO channel modeling. A short conclusion is provided in Section V.

II. FREE SPACE CHANNEL

The plane- and spherical-wave models for a (4,4) MIMO system are illustrated in Fig. 1. The plane-wave model assumes that the incident signal is a plane wave, which means the DOD (θ_T, ϕ_T) (DOA (θ_R, ϕ_R)) is the same for all the elements in the Tx (Rx). θ_T and θ_R are the azimuth angles of DOD and DOA,

respectively, while ϕ_T and ϕ_R denote the elevation angles. We assume that both the transmit and receive arrays are parallel with the horizontal plane, therefore $\phi_R = 180^\circ - \phi_T$. However, when the distance between Tx and Rx is short, or the array size is large, the waves are more appropriately considered as spherical. When spherical waves are used, the DODs and DOAs are different for each pair of transmit and receive antennas; therefore, the DODs and DOAs are represented as $(\theta_{Tij}, \phi_{Tij})$ and $(\theta_{Rij}, \phi_{Rij})$, where i and j are the indexes of the transmit and receive antennas. Assuming each antenna of an array is in the far field of the antennas of the other array, and that the antenna elements are isotropic, the channel response h between any two antennas is calculated according to the formula

$$h \propto \frac{e^{-j\frac{2\pi D}{\lambda}}}{D} \quad (1)$$

where λ is the wavelength of the carrier, and D is the distance between the transmit and receive antenna pair. In this section, we assume the LOS is the only path in the channel. The open-loop capacity is calculated by [1]

$$C = \log_2 \left| I_{n_R} + \left(\frac{\text{SNR}}{n_T} \right) \cdot \mathbf{H}\mathbf{H}^\dagger \right| \quad (2)$$

where n_T and n_R are the numbers of antennas at the transmitter and receiver sites, respectively, \mathbf{H} is the MIMO complex channel matrix normalized such that its Frobenius norm is $n_T n_R$, SNR is the average signal-to-noise ratio over the receive antennas, and \dagger stands for the complex conjugate transpose of the matrix. Using the plane-wave model in free space, the calculated capacity of the (4,4) MIMO system is $\log_2 [1 + \text{SNR} \times n_R] = 8.65$ b/s/Hz for an SNR of 20 dB, no matter how the DOA, DOD, the antenna spacing, and the array geometries are changed, because the rank of the matrix is one. On the other hand, the maximum capacity is $\min(n_T, n_R) \log_2 [1 + (\text{SNR} \times n_R / \min(n_T, n_R))]$; this occurs when the channel matrix is orthogonal with equal eigenvalues. For the (4,4) case, this maximum is 26.6 b/s/Hz for SNR = 20 dB. In the following subsections, we show that the maximum capacity is reached in free space over distances typically found in WLAN applications using the more precise spherical-wave model.

A. Azimuth Angle of DOA and DOD

Let both arrays be in the same horizontal plane ($\phi_T = \phi_R = 90^\circ$), and let the distance between the midpoints of Tx and Rx, denoted as the T-R distance, be 100λ . The MIMO capacities calculated using the spherical-wave model are shown in Fig. 2 for various azimuth angles of DOA, DOD, and for two values of antenna spacing. First, we observe that this capacity varies with DOA and DOD. With the spherical-wave model, the low-capacity values are achieved when at least one of θ_T and θ_R are -90° or 90° . On the other hand, for 1λ , we find that the maximum capacity occurs when the arrays are broadside to each other, or when $\theta_T = \theta_R = 0^\circ$. Also, capacity increases with antenna spacing. The maximum capacity at spacing equal to 1λ is almost 10.1 b/s/Hz, which is 1.5 b/s/Hz larger than that of the plane-wave model. When the spacing approaches 5λ (not shown in the figure), the capacity achieves that of a full-rank channel matrix, 26.63 b/s/Hz, which is 18 b/s/Hz larger

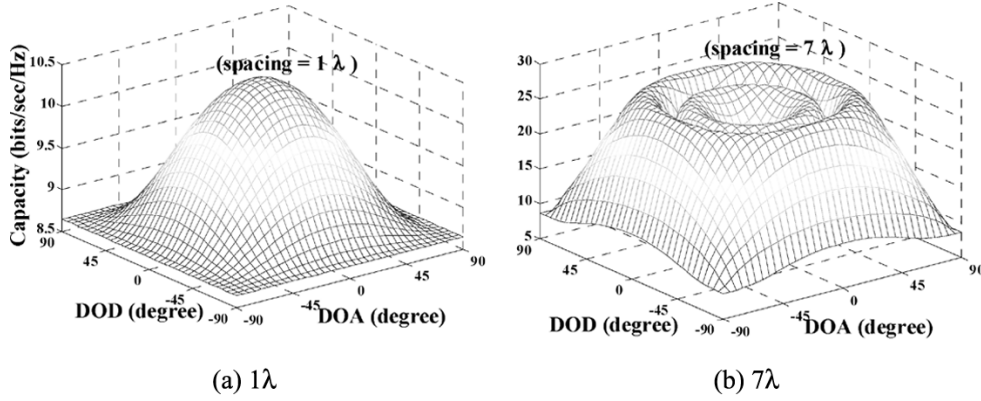


Fig. 2. Change of MIMO capacity with DOA and DOD. The T-R distance is 100λ , and the SNR is 20 dB. (a) Antenna spacing = 1λ . (b) Antenna spacing = 7λ .

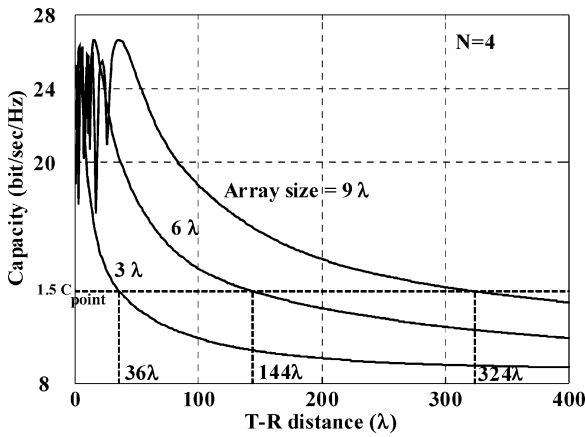


Fig. 3. Capacity versus array size and T-R distance. The threshold distances that determine the appropriateness of the plane-wave model.

than the capacity of the plane-wave model. When the spacing is less than 5λ , the maximum capacity corresponds to the angles $(\theta_T, \theta_R) = (0^\circ, 0^\circ)$. When the spacing exceeds 5λ , the maximum is no longer at $(0^\circ, 0^\circ)$, as shown in Fig. 2(b), but the ripples still reach the maximum capacity. The distribution of the capacity is symmetric about the point $(\theta_T, \theta_R) = (0^\circ, 0^\circ)$.

A distance threshold that determines when the spherical-wave model should be used can be determined empirically. We identify the threshold distance R_{th} , below which the capacity of the spherical-wave model is greater than 1.5 times the plane-wave model for a given array size. In other words, the capacity underestimation error is 50% at this distance when the plane-wave model is used, and this error increases dramatically when the T-R distance is shorter than R_{th} . From the above discussion, we have realized that the maximum discrepancy between the plane- and spherical-wave models usually corresponds to the arrays being broadside to each other. Therefore, this is the geometry considered next. As shown in Fig. 3, for the array sizes 3λ , 6λ , and 9λ , the corresponding threshold distances are 36λ , 144λ , and 324λ , respectively, in the simulation when the number of antennas is four. The relationship that fits this data is $R_{th} = 4L^2$, where L is the array size in units of wavelength. Given the formula $R_{th} = \alpha L^2$, the value of α ranges from 3.75 to 4.4 for the number of antennas ranging between 3 and 16. Therefore, $4L^2$ is a reasonable threshold distance.

It is interesting to note that this threshold distance to distinguish the plane- and spherical-wave models is similar to the threshold $R = 2L^2$, which marks the boundary between the Fresnel and the Fraunhofer (far-field) zone, where L denotes the antenna size in this case [15]. This threshold is determined under the constraint that the maximum phase deviation of the received signal between any two points of the antenna is less than $\pi/8$ [15].

The formula for the threshold distance, $R_{th} = 4L^2$, may be generalized by considering a conventional beamforming perspective. The basic idea is that the channel rank will exceed unity when any pair of elements in one of the arrays can be resolved by the other array. Below, we will use the outer two elements. The resolving capability of an array relates to the beamwidth of its antenna pattern with all-unity weights. The beamwidth of a uniformly weighted array is the same as that of a uniformly illuminated continuous aperture of the same size [16]. Therefore, the resolving capability of an array depends only on its aperture size, and not on how many antenna elements fill the aperture.

The normalized broadside radiation pattern of a line source of length L (in units of wavelength) is [16]

$$f(\Theta) = \frac{\sin(L\pi \sin \Theta)}{L\pi \sin \Theta}. \quad (3)$$

Assuming the transmit array size is L_T , the half-power beamwidth of the transmit array is

$$\Theta_{3 \text{ dB}} \approx \frac{0.886}{L_T}. \quad (4)$$

The T-R distance R , such that the receive array with array size L_R is entirely within the 3 dB beamwidth, satisfies

$$\begin{aligned} L_R &\leq 2R \sin \frac{\Theta_{3 \text{ dB}}}{2} \approx R \Theta_{3 \text{ dB}} \approx \frac{0.886R}{L_T} \\ \Rightarrow R &\geq 1.13L_R L_T. \end{aligned} \quad (5)$$

This distance, denoted as $R_{3 \text{ dB}}$, is less than the empirical threshold distance R_{th} . This tells us that the half-power beamwidth is too large to determine the threshold distance, because the underestimation of channel capacity is over 100% at $R_{3 \text{ dB}}$.

The beamwidth that matches $R_{th} = 4L^2$ is

$$\Theta_{th} = \frac{0.25}{L_T} \approx \Theta_{0.225 \text{ dB}}. \quad (6)$$

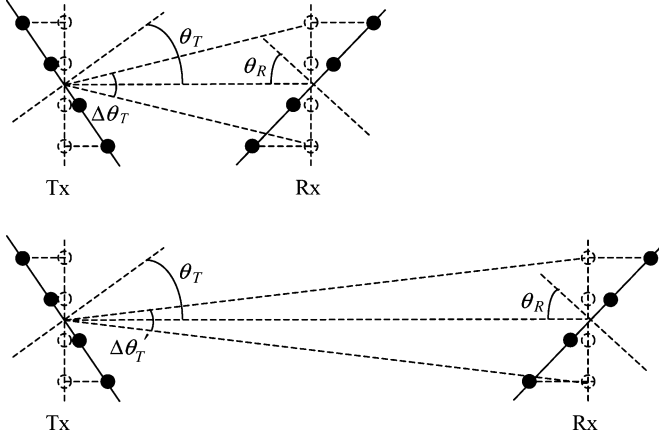


Fig. 4. How rotation of arrays and longer range affects the subtended angle $\Delta\theta_T$.

Therefore, the threshold distance R_{th} is that distance such that the receive array subtends the angle $\Theta_{0.225 \text{ dB}}$, which is the 0.225 dB-down beamwidth of the transmit array. The formula can be generalized to the situation when the transmit and receive array sizes are not equal, i.e.,

$$R_{\text{th}} \approx R_{0.225 \text{ dB}} = 4L_T L_R. \quad (7)$$

This formula can be further generalized to apply to arrays that are not broadside to each other. We observe that a beam from a uniformly illuminated aperture of length L_T (wavelengths), scanned to an angle θ_T from boresight (i.e., from the broadside direction), has a 3-dB beamwidth $0.886/(L_T \cos \theta_T)$ [16]. This is equivalent to substituting L_T in (4) with the effective aperture size presented to the θ_T direction $L_T \cos \theta_T$. The transmitter effective aperture size is illustrated in Fig. 4 by the length of the array of dashed circles at the transmitter end.

Similarly, a linear receive array which is rotated an angle θ_R away from the broadside orientation subtends a smaller angle $\Delta\theta_T$, as viewed from the transmit array, and is therefore more likely to fall within the threshold angle. Therefore, (7) may be further generalized to

$$R_{\text{th}} = 4L_T L_R \cos \theta_T \cos \theta_R. \quad (8)$$

For example, when two arrays are perpendicular to each other, or when they are at the endfire side of each other, the distance R_{th} is equal to 0, because at least one of the DOAs or DODs is equal to 90° . In that case, the plane-wave model is appropriate for any distance, and the channel capacity achieves the minimum value. Finally, Fig. 4 shows how the longer range of the lower drawing causes $\Delta\theta_T$ to be smaller than $\Delta\theta_T$ of the upper drawing, which shows why the plane-wave model is appropriate for long range.

Although not tested specifically in this paper, nonlinear arrays are conjectured to have the same threshold distance as (7), with L_T and L_R replaced by the effective aperture lengths of the transmit and receive arrays as presented to the directions of each other.

Next, we consider the minimum element spacing to achieve the maximum capacity in the context of beams [17]. With an N -element uniform linear array (ULA), in total, N orthogonal

beams can be formed, and the directions of the beams θ_i , $i = 1, 2, \dots, N$, satisfy

$$\sin \theta_i = \frac{(i - \frac{N+1}{2})}{Nd} \quad (9)$$

where d is the element spacing in the unit of wavelength [16]. Each beam has its peak gain where the gains of other beams are equal to 0. Therefore, if N receive antennas are placed, respectively, in the directions of the orthogonal beams formed by the transmit array, the channel matrix is close to $N\mathbf{I}$, where \mathbf{I} is the identity matrix [17]. Assuming the element spacings of the transmit array and the receive arrays are d_T and d_R in units of wavelength, respectively, and assuming each receive antenna is placed in the direction of a different orthogonal beam, we have

$$\begin{aligned} \sin \theta_N &= \sin \left(\frac{\Delta\theta}{2} \right) = \frac{(N-1)}{2Nd_T} = \frac{\frac{(N-1)d_R}{2}}{\sqrt{R^2 + \left(\frac{(N-1)d_R}{2} \right)^2}} \\ \Rightarrow d_R &= \frac{2R}{\sqrt{(2Nd_T)^2 - (N-1)^2}}. \end{aligned} \quad (10)$$

When $d_T \gg ((N-1)/2N)$, the receive element spacing d_R can be approximated by

$$d_R \approx \frac{R}{Nd_T}. \quad (11)$$

For example, when $R = 100$, $N = 4$, and $d_T = d_R$, the minimum receive element spacing to achieve the full rank is 5λ , which is consistent with our previous simulation result.

When MIMO is applied to the indoor WLAN using four antennas with the center frequency at 5.8 GHz, the threshold distances are around 1.86, 7, and 16.8 m for the antenna spacings of 1λ , 2λ , and 3λ , respectively. This indicates that the spherical-wave model should be used, and antenna spacings in excess of 1λ should be considered for MIMO in indoor WLAN applications where the client platform, such as a laptop computer or flat-panel TV, might support larger element spacings.

B. Elevation Angle

Since MIMO capacity depends on the differences among the DOAs and the differences among the DODs for different elements, the performance can be affected by changing the elevation angle, which is defined as the angle between the LOS path and Z axis, as shown in Fig. 1. For example, when the arrays are at the endfire side of each other, i.e., the azimuth angles $(\theta_T, \theta_R) = (-90^\circ, -90^\circ)$ and the elevation angles $\phi_T = \phi_R = 90^\circ$ (Tx and Rx on the same plane), the system has minimum capacity. As the elevation angle grows from this point, the relative geometry between the arrays is the same as though both arrays were in the same horizontal plane, and the azimuth angles were following the $\theta_T = \theta_R$ line in Fig. 2. This implies that increasing the elevation angle corresponds to an increase in capacity.

The previous azimuth variations do not capture relative twists between the arrays. Fig. 5 shows the capacity when $\phi_T = 0^\circ$ (i.e., when one array is directly above the other) for various relative azimuth angles. In the simulation, the θ_R is fixed at 90° , and the θ_T varies from -90 to 90° . For all four antenna spacings, the minimum channel capacity occurs at $\theta_T = 0^\circ$, i.e.,

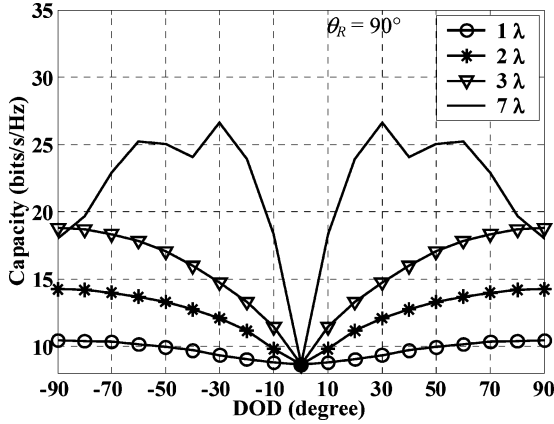


Fig. 5. Impact of elevation angle to the MIMO system with different antenna spacing. The azimuth DOA is fixed at 0° , the T-R distance is 100λ , and the SNR is 20 dB.

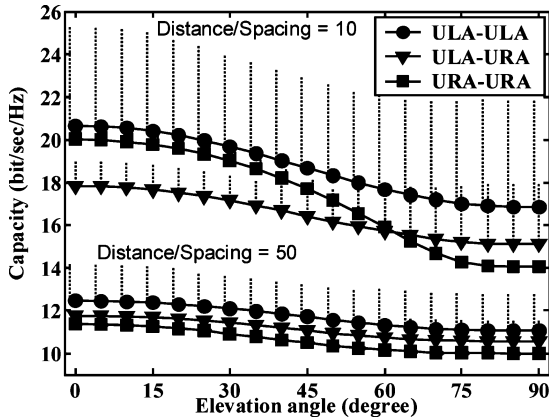


Fig. 6. Average and standard deviation of MIMO capacity of different array geometries. The distance-to-spacing ratios are 50 and 10.

when Tx and Rx arrays are orthogonal to each other. The average capacities, when the average is taken over all values of θ_T (i.e., DOD), are 9.7, 12.5, 15.8, and 21.9 b/s/Hz for 1, 2, 3, and 7λ , respectively. Comparing these with the corresponding average capacities of 8.6, 8.6, 8.7, and 9.9 b/s/Hz when the elevation angle $\phi_T = 90^\circ$, the improvement ranges from 12.8% to 121.2%, increasing with antenna spacing. Since the channel capacity is dominated by the LOS when it is available, the results suggest that the access point should be placed on the ceiling, and element spacing should be several wavelengths to increase the performance of the MIMO system.

C. Array Geometry

The MIMO capacity also changes with the array shape in free space when the spherical-wave model is used. For instance, the channel with $(\theta_T, \theta_R) = (-90^\circ, -90^\circ)$ is the same as $(\theta_T, \theta_R) = (0^\circ, 0^\circ)$ when the transmitter and receiver are uniform rectangular arrays (URAs); however, these two conditions correspond to the maximum and minimum capacity when the ULAs are employed instead. In Fig. 6, we compare the performance of links with different combinations, including ULA-ULA, ULA-URA, and URA-URA. Because of the reciprocity of the MIMO channels, the performance of URA-URA

is the same as for ULA-URA. The SNR is 20 dB, the element spacing is 2λ , and two ranges are considered, which yield T-R distance-to-element-spacing ratios of 50 and 10, as indicated in Fig. 6. The average and standard deviation of the capacity are derived assuming the DOA and DOD are independent random variables, and both uniformly distributed over $[-90^\circ, 90^\circ]$. In Fig. 6, the length of the vertical line on each curve represents the standard deviation for the corresponding array arrangement and elevation angle.

First we notice that the average capacities of the arrays with small distance-to-spacing-ratio are higher than that of the arrays with the larger ratio. The ULA-URA combination has the best average capacity for all cases, but its standard deviation is also the largest. The average capacity of URA-URA surpasses ULA-URA at most elevation angles when the distance-to-spacing ratio is 10 (i.e., for the shorter ranges). In all cases, the capacity achieves its maximum when the elevation angle ϕ_T is close to 0° . The elevation-angle effect is more significant when the distance-to-spacing ratio is smaller. For example, when the distance-to-spacing ratio is 10, the maximum variation of the average capacity is about 6 b/s/Hz for the URA-URA system. In addition, URA-URA has the feature of smallest variance, compared with the other two combinations. In other words, the performance of URA-URA is more robust to relative rotation of the arrays. Finally, we note that on the average, element spacing improves the URA-URA channel by about the same amount, 10 b/s/Hz, at the zero elevation, as it does the ULA-ULA configuration.

III. CHANNELS WITH MULTIPATH

In the previous section, we considered the capacity of the MIMO link when the LOS is the only path in the channel. However, in reality, there are multiple paths caused by the reflection, refraction, and scattering of the objects around the antennas. In this section, we compare the plane- and spherical-wave models in a square room using two-dimensional (2-D) ray tracing with the image method [18]. The reflection coefficient ρ of the walls can be expressed as [13], [19]

$$\rho = \frac{\sqrt{\varepsilon - \sin^2 \theta} - \varepsilon \cos \theta}{\sqrt{\varepsilon - \sin^2 \theta} + \varepsilon \cos \theta} \quad (12)$$

where ε is the relative permittivity of the wall, and θ is the incident angle. This formula assumes the antenna is vertically polarized. In the simulation, we assume $\varepsilon = 5$ and the room size is $(160 \times 160)\lambda$. The SNR is 20 dB. When the frequency is 5.8 GHz, the room size is about $(8 \text{ m} \times 8 \text{ m})$, which is the size of a typical office. Both Tx and Rx are four-element ULAs, and they are located at random and in the same horizontal plane in the room. The orientation of the array is also uniformly distributed in azimuth over $[-90^\circ, 90^\circ]$. With up to n times of reflection, the total number of reflected paths is equal to $2n(n+1)$. In our simulation, up to 20 reflections are considered, so the number of total paths is 840. The number of trials in the simulation is 5000. Fig. 6 shows the average capacities for normalized channel matrices with the plane- and spherical-wave models. As illustrated in Fig. 7, the discrepancy between these two models is negligible when the antenna spacing is less than one wavelength, but the

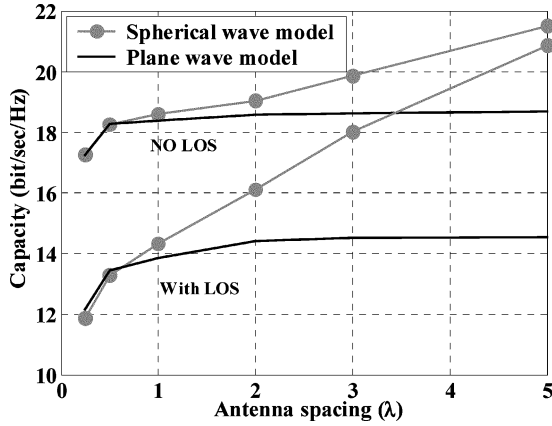


Fig. 7. Comparison of the average capacities.

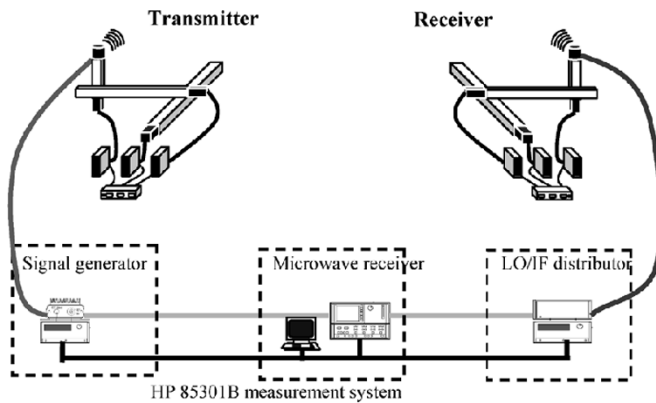


Fig. 8. Overview of MIMO channel-measurement system.

error increases with the antenna spacing. We observe the difference of the average capacity is about 3 b/s/Hz at 5λ when LOS is not included. If the LOS is included in the simulations, bringing the total number of paths to 841, the discrepancy increases to 6.2 b/s/Hz. In the plane-wave model, the average capacity tends to saturate when the antenna spacing exceeds 1λ , whereas in the spherical-wave model, the performance improves continuously for antenna spacing up to 5λ . The antenna spacings beyond 5λ are not considered in the simulation, because large array size restricts the array locations to a very small area of the room.

IV. VALIDATION WITH MEASUREMENT

Next, we use measured data acquired in the Smart Antenna Research Laboratory (SARL) at the Georgia Institute of Technology to compare the capacities of measured channels and the channels reconstructed with both plane- and spherical-wave models based on the estimated parameters. The testbed, illustrated in Fig. 8, is composed of two parts: 1) the 3-D actuator system, which moves the antenna to preprogrammed locations to form a virtual array (there are two of these systems, one at each end of the link); and 2) the HP85301B antenna-pattern measurement system, which captures the frequency response of the channel. The HP85301B is a high-precision measurement system with a dynamic range of 89 dB in our band of operation. The details of the measurement system are provided in [5].

The measurements were taken in the main room of the SARL, which is approximately $7 \times 4 \times 3 \text{ m}^3$, and which contains desks

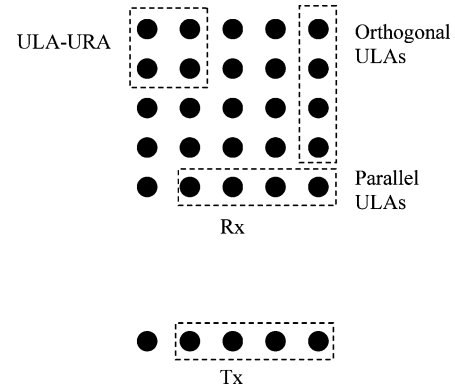


Fig. 9. Extraction of three different subarrays: 1) parallel ULAs; 2) orthogonal ULAs; and 3) ULA-URA.

and 1.5 m-high partitions. The T-R distance was 2.56 m, and the link was in the center of the open area. In the experiment, two separate measurements were conducted; one for parameter estimation, and the other for direct capacity measurement. In the path parameter estimation, the arrays at both ends are $(4 \times 4 \times 3)$ uniform cubicle arrays with antenna spacing 0.48λ at 5.8 GHz. In the sequel, λ always corresponds to 5.8 GHz. 401 samples are measured from 5.55–6.05 GHz with the stepped-frequency method to achieve the temporal resolution of 2 ns. Spatial and frequency smoothing is achieved by averaging the correlation matrices of the subarrays [20], [21]. The subarray size used in the estimation is $(3 \times 3 \times 2)$ for both DOA and DOD. The delay is estimated by unitary estimation of signal parameters via the rotational invariance technique (ESPRIT), and the DOA and DOD are jointly estimated by multidimensional ESPRIT [5], [22], [23]. According to the parameter-estimation results, the channel is dominated by the LOS component and the single-bounce paths reflected from the walls. The power of the LOS component is 10 dB stronger than the second-strongest path.

In the capacity measurement, the Tx array is a five-element ULA, while the Rx array is a (5×5) URA. The measurements with five different element spacings (0.25, 0.5, 1, 2, 3 λ) are conducted at each location. To obtain multiple outcomes for the flat-fading capacity cumulative distribution function (CDF), the frequency spacing is set to 10 MHz. Our measurement result shows that with a 10-MHz separation, the correlation coefficient between adjacent frequency samples is less than 0.4. Accordingly, there are 51 samples of the flat-fading channel over the 500-MHz bandwidth. We consider that 51 different frequency samples for the same MIMO antenna locations represent 51 approximately independent outcomes of the MIMO channel. To get spatial samples of capacity, subarrays with different array shapes and spacings are extracted from the five-element ULA and (5×5) URA, as shown in Fig. 9. For different element spacings, the five-element ULA and (5×5) URA are simply scaled so that the nearest neighbors have the specified spacing. We note that the spatial samples of the MIMO channel, especially for the 0.25λ spacing, are probably correlated. With this arrangement, we may extract a total of 1632 outcomes of MIMO channel matrices when the (Tx, Rx) subarray setting is the $(4, 2 \times 2)$ ULA-URA combination, and 1020 outcomes when the setting is $(4, 4)$ ULA-ULA for capacity CDF calculation. When

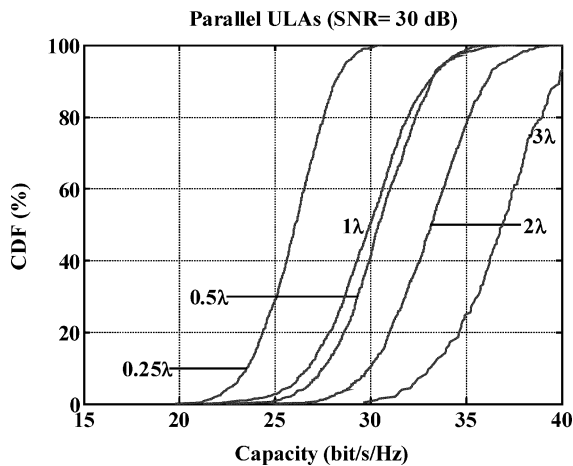


Fig. 10. Measured MIMO capacity of parallel ULAs when SNR = 30 dB.

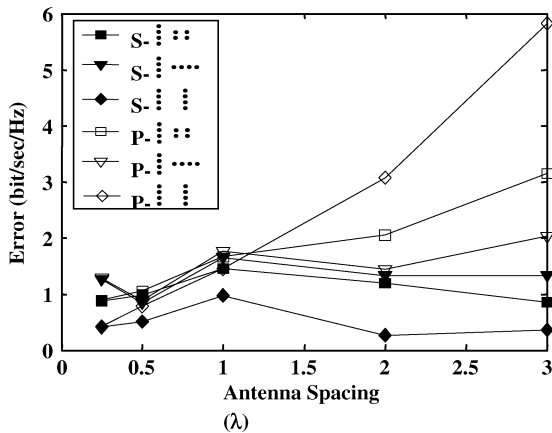


Fig. 11. Comparison of measured and estimated capacities. Difference between the mean capacities of the directly measured and reconstructed channels.

the array arrangement is ULA–ULA, the Tx and Rx can be either orthogonal or parallel; accordingly, we may measure the channel capacities of three different array geometries.

The CDFs of the directly measured capacities of the (4,4) ULA–ULA MIMO system, with the arrays broadside to each other for various antenna spacings, are shown in Fig. 10. We observe that when the antenna spacing is increased from 0.5λ to 3λ , the S-shaped CDFs move to the right by about 7 b/s/Hz, corresponding to an increase in the median capacity of about 23%.

The parameters estimated from the first set of measurements were used to reconstruct the channel matrices of various geometries using both the plane- and spherical-wave models. The resulting CDFs as functions of spacing have the same S-shapes as the CDFs of the directly measured capacities, however, they are translated horizontally to generally different positions, and therefore, they have different mean capacities. Fig. 11 shows the mean capacity for the directly measured channels minus the mean capacity of the reconstructed channel as a function of the LOS model (S for spherical or P for plane) and the array geometries. The array geometries considered include the (4, 2×2) systems and the (4,4) MIMO systems, where the ULAs at both ends are either parallel or orthogonal to each other. In all

cases, the difference increases with the antenna spacing when the plane-wave model is used, while the difference is maintained at a low level for various antenna spacings when the spherical-wave model is applied. We observe that the plane-wave model obviously underestimates the measured capacity when the antenna spacing is 1λ or larger. When the antenna spacing is 3λ , error in capacity resulting from use of the plane-wave model is as large as 6 b/s/Hz. In contrast, the estimated capacity based on the spherical-wave model has much better agreement with the measured capacity.

V. CONCLUSIONS

In this paper, we have considered the pure LOS channel as well as multipath channels based on ray-tracing methods and on measurements. We have shown that when the LOS is present, the spherical-wave model is more appropriate than the plane-wave model for MIMO systems when the T-R distance is short or the antenna spacing is large. A threshold distance is determined empirically and generalized using beamspace arguments. We also show that, unlike the plane-wave model, the spherical-wave model enables the performance of the short-range LOS MIMO system to be significantly improved by properly adjusting the DOA, DOD, and the array geometries. In particular, capacity can be dramatically improved by increasing the antenna spacing at both ends of the link. According to the simulations, better capacity can be achieved by placing the base station on the ceiling, provided the LOS is available. The results suggest that greater-than-single wavelength element spacing should be considered for nonhandheld user platforms, such as the applications of WLAN. There are several topics suggested for future research. Those include performance of the short-range MIMO link for wide bandwidth and when polarization variation is considered. The effects of path loss could be considered as range varies. Finally, 3-D-multipath diffraction effects could be considered.

REFERENCES

- [1] G. J. Foschini and M. J. Gans, "On limits of wireless communications in a fading environment when using multiple antennas," *Wireless Pers. Commun.*, pp. 311–335, 1998.
- [2] G. G. Raleigh and J. M. Cioffi, "Spatio-temporal coding for wireless communication," *IEEE Trans. Commun.*, vol. 46, no. 3, pp. 357–366, Mar. 1998.
- [3] D.-S. Shiu, G. J. Foschini, M. J. Gans, and J. M. Kahn, "Fading correlation and its effect on the capacity of multielement antenna systems," *IEEE Trans. Commun.*, vol. 48, no. 3, pp. 502–513, Mar. 2000.
- [4] D. Chizhik, G. J. Foschini, M. J. Gans, and R. A. Valenzuela, "Keyholes, correlations, and capacities of multielement transmit and receive antennas," *IEEE Trans. Wireless Commun.*, vol. 1, no. 2, pp. 361–368, Mar. 2002.
- [5] J.-S. Jiang, "Measurement, modeling, and performance of indoor MIMO channels," Ph.D. dissertation, Georgia Inst. Technol., Atlanta, GA, 2004.
- [6] P. F. Driessen and G. J. Foschini, "On the capacity formula for multiple-input multiple-output wireless channels: A geometric interpretation," *IEEE Trans. Commun.*, vol. 47, no. 2, pp. 173–176, Feb. 1999.
- [7] P. Kyritsi, "MIMO capacity in free space and above perfect ground: Theory and experimental results," in *Proc. IEEE Symp. Pers., Indoor, Mobile Radio Commun.*, vol. 1, Sep. 2002, pp. 182–186.
- [8] A. Hutter, F. Platbrood, and J. Ayadi, "Analysis of MIMO capacity gains for indoor propagation channels with LOS component," in *Proc. IEEE Symp. Pers., Indoor, Mobile Radio Commun.*, vol. 3, Sep. 2002, pp. 1337–1341.

- [9] D. Chizhik, F. Rashid-Farrokh, J. Ling, and A. Lozano, "Antenna separation and capacity of BLAST in correlated channels," in *Proc. IEEE Antenna Propag. Wireless Commun. Conf.*, 2003, pp. 183–185.
- [10] K.-H. Li, M. A. Ingram, and A. V. Nguyen, "Impact of clustering in statistical indoor propagation models on link capacity," *IEEE Trans. Commun.*, vol. 50, no. 4, pp. 521–523, Apr. 2002.
- [11] L. Schumacher, K. I. Pedersen, and P. E. Mogensen, "From antenna spacings to theoretical capacities—Guidelines for simulating MIMO systems," in *Proc. 13th IEEE Int. Symp. Pers., Indoor, Mobile Radio Commun.*, vol. 2, Sep. 2002, pp. 587–592.
- [12] C.-N. Chuah, G. J. Foschini, R. A. Valenzuela, D. Chizhik, J. Ling, and J. M. Kahn, "Capacity growth of multi-element arrays in indoor and outdoor wireless channels," in *Proc. IEEE Wireless Commun. Netw. Conf.*, vol. 3, 2000, pp. 1340–1344.
- [13] A. Burr, "Evaluation of capacity of indoor wireless MIMO channeling using ray tracing," in *Proc. IEEE Int. Seminar Broadband Commun.*, 2002, pp. 28-1–28-6.
- [14] V. Pohl, V. Jungnickel, T. Haustein, and C. V. Helmolt, "Antenna spacing in MIMO indoor channels," in *Proc. IEEE Veh. Technol. Conf.*, vol. 2, Spring 2002, pp. 749–753.
- [15] D. T. Paris, *Basic Electromagnetic Theory*. New York: McGraw-Hill, 1969.
- [16] R. J. Mailloux, *Phased Array Antenna Handbook*. Norwood, MA: Artech House, 1994.
- [17] M. A. Ingram, "Measurement, modeling and performance of the MIMO channel," in *Adaptive Antenna Arrays: Trends and Applications*, S. Chandran, Ed. New York: Springer-Verlag, Jun. 2004, pp. 616–624.
- [18] M. C. Lawton and J. P. McGeehan, "The application of a deterministic ray launching algorithm for the prediction of radio channel characteristics in small-cell environment," *IEEE Trans. Veh. Technol.*, vol. 43, no. 6, pp. 955–969, Nov. 1994.
- [19] S. R. Saunders, *Antennas and Propagation for Wireless Communication Systems*. New York: Wiley, 1999.
- [20] J. E. Evans, J. R. Johnson, and D. F. Sun, "Applications of advanced signal processing techniques to angle of arrival estimation in ATC navigation and surveillance systems," MIT, Lincoln Lab. Tech. Rep., 1982.
- [21] T.-J. Shan, A. A. Paulraj, and T. Kailath, "On smoothed rank profile tests in eigenstructure methods for directions-of-arrival estimation," *IEEE Trans. Acoust., Speech, Signal Process.*, vol. ASSP-35, no. 10, pp. 1377–1385, Oct. 1987.
- [22] M. Haardt and J. A. Nosssek, "Unitary ESPRIT: How to obtain increased estimation accuracy with a reduced computational burden," *IEEE Trans. Signal Process.*, vol. 43, no. 5, pp. 1232–1242, May 1995.
- [23] M. Haardt and J. A. Nosssek, "Simultaneous Schur decomposition of several nonsymmetric matrices to achieve automatic pairing in multi-dimensional harmonic retrieval problems," *IEEE Trans. Signal Process.*, vol. 46, no. 1, pp. 161–169, Jan. 1998.



Jeng-Shiann Jiang (S'98–M'05) was born in Tainan City, Taiwan, R.O.C. He received the B.S. and M.S. degrees in electrical engineering from National Sun Yat-Sen University, Kaohsiung, Taiwan, R.O.C., in 1992 and 1994, respectively, and the M.S. and Ph.D. degrees in electrical and computer engineering from the Georgia Institute of Technology, Atlanta, in 2000 and 2004, respectively.

From 1996 to 1997, he was a Hardware Circuit Design Engineer with D-Link Network Corporation, responsible for the circuit design of IEEE 802.3 Fast Ethernet adapters. From 1997 to 1998, he was a Software Engineer with the Industrial Technology Research Institute (ITRI), Taiwan, R.O.C. From 1999 to 2000, he was a Teaching Assistant with the School of Electrical and Computer Engineering, Georgia Institute of Technology. From 2000 to 2004, he has been a Research Assistant with the Smart Antenna Research Laboratory, Georgia Institute of Technology. His research interests include MIMO technology, wireless channel measurement and modeling, parameter estimation, orthogonal frequency-division multiplexing, error-control coding, and space-time techniques.



Mary Ann Ingram (S'84–M'85–SM'03) received the B.E.E. and Ph.D. degrees from the Georgia Institute of Technology (Georgia Tech), Atlanta, in 1983 and 1989, respectively.

From 1983 to 1986, she was a Research Engineer with the Georgia Tech Research Institute, Atlanta, performing studies on radar electronic countermeasure (ECM) systems. In 1986, she became a Graduate Research Assistant with the School of Electrical and Computer Engineering, Georgia Tech, where in 1989, she became a Faculty Member and is currently a Professor. Her early research areas were optical communications and radar systems. In 1997, she established the Smart Antenna Research Laboratory (SARL) at Georgia Tech, which emphasizes the application of multiple antennas to wireless communication systems. The SARL performs system analysis and design, channel measurement, and prototyping relating to a wide range of wireless applications, including wireless local area network and satellite communications, with focus on the lower layers of communication networks.